

Behaviour and design of Grade 10.9 high-strength bolts under combined actions

Dongxu Li*, Brian Uy^a, Jia Wang^b and Yuchen Song^c

School of Civil Engineering, The University of Sydney, NSW 2006, Australia

(Received June 10, 2019, Revised February 9, 2020, Accepted February 13, 2020)

Abstract. The use of high-strength steel and concrete in the construction industry has been gaining increasing attention over the past few decades. With it comes the need to utilise high-strength structural bolts to ensure the design load to be transferred safely through joint regions, where the space is limited due to the reduced structural dimensions. However, research on the behaviour of high-strength structural bolts under various loading combinations is still insufficient. Most of the current design specifications concerning high-strength structural bolts were established based on a very limited set of experimental results. Moreover, as experimental programs normally include limited design parameters for investigation, finite element analysis has become one of the effective methods to assist the understanding of the behaviour of structural components. An accurate and simple full-range stress-strain model for high-strength structural bolts under different loading combinations was therefore developed, where the effects of bolt fracture was included. The ultimate strength capacities of various structural bolts obtained from the present experimental program were compared with the existing design provisions. Furthermore, design recommendations concerning the pure shear and tension, as well as combined shear and tension resistance of Grade 10.9 high-strength structural bolts were provided.

Keywords: high-strength bolts; Grade 10.9; combined tension and shear; numerical simulation; fracture; design codes

1. Introduction

Over the past few decades, there has been an emerging trend to use high-strength materials in the construction industry, which has allowed the dimensions and self-weight of structural elements to be reduced, and the concept of sustainable building structures to be promoted (Uy 2001, Zhao and Yuan 2010, Du *et al.* 2017, Shamass and Cashell 2017, Ma *et al.* 2018, Wang and Sun 2019, Huang *et al.* 2019, Li *et al.* 2019, Wang *et al.* 2020). However, with the application of high-strength materials, the joint regions between connected elements also become limited (Ebrahimi *et al.* 2019, Cai and Young 2019). To ensure the load can be transferred safely within the limited space, the use of higher strength structural bolts provides an ideal solution (Coelho *et al.* 2004, Coelho and Bijlaard 2007, Li *et al.* 2019).

In recent years, high-strength bolts have received increasing attention in design and construction, owing to their significant structural and economic benefits. Many of the current international design standards have allowed the utilisation of high-strength bolts. In particular, high-strength

bolts with grade up to 10.9 have been included into the European and American Standards (Eurocode 3, 2005, AISC-360, 2016); whilst the Australian Standards just allowed high-strength bolts of Grade 8.8 to be adopted (AS4100, 2016). It is noteworthy that high-strength bolts can be designed based on both bearing- and slip-resistant requirement. For those that were designed with the slip-resistant requirement, a certain amount of preloading (normally 70% of the proof strength) was required (Nah and Choi 2017). The Eurocode 3 (2005) and EN 14399 (2005) have included two types of preloadable high-strength bolts of different properties and standardised products. According to their failure modes under axial tension, these high-strength bolts can be categorised as HR (British system) and HV (German system) bolts. Considering the less favoured strength capacity and ductility of HV bolts, most of the high-strength bolts in the current Australian market were limited to HR bolts of Grade 8.8.

As one of the major structural components, the mechanical properties of high-strength bolts are of significant interest in civil engineering. Against this background, Sterling and Fisher (1964), Nair *et al.* (1974) and Amrine and Swanson (2004) tested the tensile performance of ASTM-A490 bolts, which possessed similar mechanical properties with Grade 10.9 bolts, and compared the test results with American Standards. On this basis, a few European scholars investigated the behaviour of Grade 10.9 bolts under pure tension and shear, with studies by Lange and González (2012), D'Aniello *et al.* (2016) and Ketabdari *et al.* (2019). In addition to the studies on the structural bolts, shear capacities of headed studs have been performed extensively, with studies by EI-Lobody and Lam

*Corresponding author, Research Associate

E-mail: dongxu.li@sydney.edu.au

^a Professor

E-mail: brian.uy@sydney.edu.au

^b Research Associate

E-mail: jia.wang@sydney.edu.au

^c Ph.D. Student

E-mail: yuchen.song@sydney.edu.au

(2002), Hou *et al.* (2012), Ding *et al.* (2017), Qi *et al.* (2017), Yan *et al.* (2018). However, structural bolts in engineering practice might be subjected to both tension and shear at joint regions. Moreover, such combined effects are also common in wind-bracing fasteners and structures. To the best knowledge of the authors, only a handful of studies looked at the strength limit state of Grade 10.9 bolts or equivalent A490 bolts under combined tension and shear (Chesso *et al.* 1965, Renner and Lange 2012, Kawohl and Lange 2016). It is noteworthy that the previous studies on Grade 10.9 bolts or equivalent A490 bolts under combined loading were limited to partial threaded bolts with hexagonal bolt heads only. To date, no experimental studies have been performed on the high-strength fully threaded set screws or partial threaded bolts with countersunk heads to investigate their performance under combined actions.

Finite element analysis has become one of the effective methods to assist the understanding of the behaviour of structural components. With this method being used, the establishment of codes of practice becomes economical and effective. Vasdravellis *et al.* (2014), Rehman *et al.* (2016) and Yang *et al.* (2017) pointed out the necessity of calibrating fracture models for structural bolts, which can

significantly improve the understanding of full-range behaviour of structural joints and frames. Pavlović *et al.* (2013), Grimsmo *et al.* (2016), Francavilla *et al.* (2016), Hu *et al.* (2016), Long *et al.* (2016), Hedayat *et al.* (2017) and D'Aniello *et al.* (2017) developed finite element models to mirror the behaviour of high-strength bolts under axial tension and pure shear. However, the previous developed models included the bolt threads and focused on the behaviour of the bolt itself. This type of model for the structural bolt was not practical and was less computational efficient when complicated structural joints and frames were simulated. Therefore, it is imperative to develop an accurate, yet simple and full-range model for high-strength bolts under different loading conditions, where the effects of bolt fracture are also considered.

The above literature review demonstrates that studies on the behaviour of high-strength bolts of Grade 10.9 under combined actions have not been carried out sufficiently. Thus, an extensive set of tests on Grade 10.9 bolts under combined shear and tension is reported herein, through which the strength limit state behaviour of Grade 10.9 bolts with various diameters and bolt head types is determined. The present study is to investigate the ultimate strength

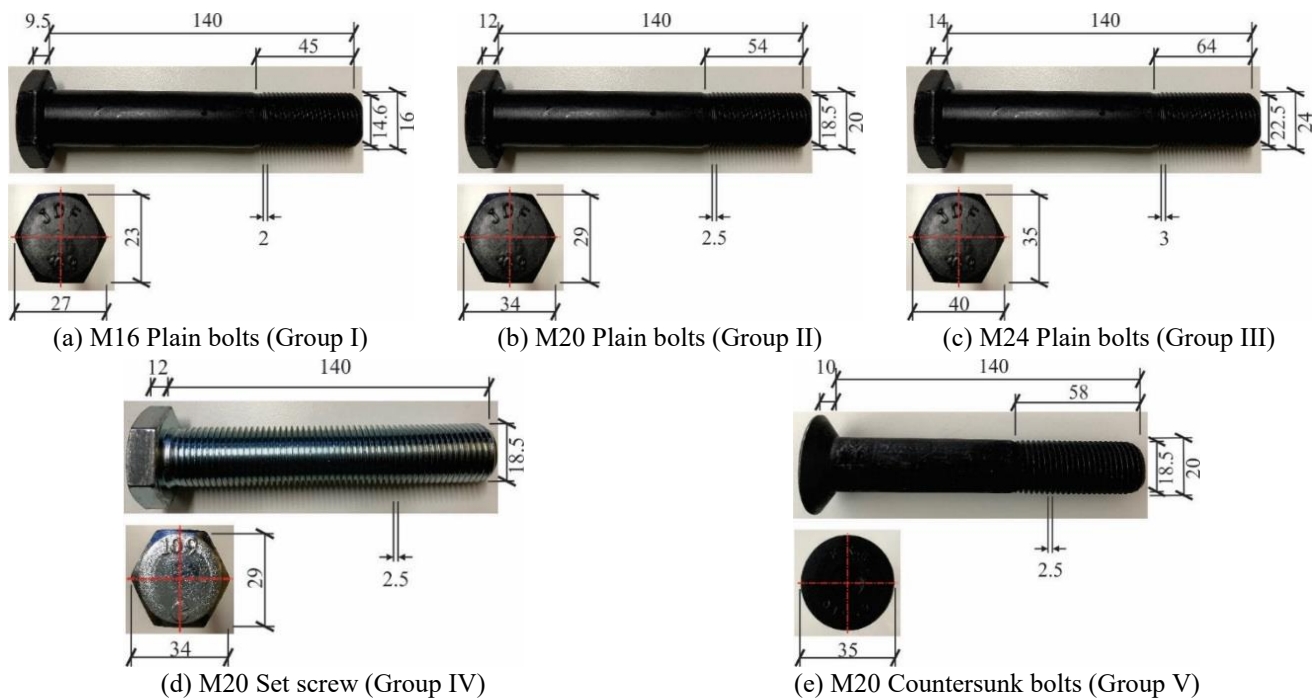


Fig. 1 Dimensions of different types of high-strength bolts of Grade 10.9

Table 1 Geometric details of test specimens

Groups	Bolt type	Nominal diameter d_0 (mm)	Thread length L_s (mm)	Total length L_0 (mm)	Thread pitch P (mm)	A (mm)	B (mm)	C (mm)	A_0 (mm ²)	A_s (mm ²)
I	Plain	16.0	45.0	140	2.0	23	27	9.5	201	157
II	Plain	20.0	54.0	140	2.5	29	34	12.0	314	245
III	Plain	24.0	64.0	140	3.0	35	40	14.0	452	353
IV	Set screw	20.0	140.0	140	2.5	29	34	12.0	314	245
V	Countersunk	20.0	58.0	140	2.5	35	-	10.0	314	245

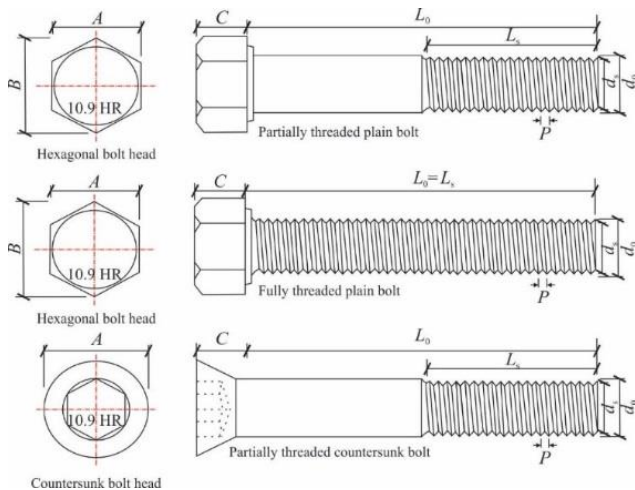


Fig. 2 Typical configuration of high-strength bolts

capacity of each bolt under various loading conditions, the effects of preloading is not within the scope of present study. In addition, simplified finite element models that include bolt fracture were developed and validated against the experimental results. The strength limit state behaviour of Grade 10.9 high-strength bolts under combined actions were compared with the current design standards, and design recommendations were thereafter suggested.

2. Experimental program

2.1 General

An experimental program consisting of 90 high-strength bolts of Grade 10.9 has been conducted according to ISO 898-1 (2009) and ASTM F606 (2016). It is noteworthy that the test methods for structural bolts under pure tension and shear have been standardised and described. However, the testing methods for structural bolts under combined tension and shear was not codified. A purpose-made testing rig, which was firstly invented by Chesson *et al.* (1965) and adapted by Renner and Lange (2012), was thereafter utilised in the present study. The tested bolts were classified into five groups, which included Group I: M16 partial threaded plain bolts; Group II: M20 partial threaded plain bolts; Group III: M24 partial threaded plain bolts; Group IV: M20 fully threaded set screws; Group V: M20 partial threaded countersunk bolts. These five groups of high-strength bolts have been tested under tension, shear and combined tension and shear without the presence of preloading, and each bolt test was repeated three times, as suggested by ISO 898-1. Configurations of the tested Grade 10.9 bolts are shown in Figs. 1 and 2, and the geometric details are summarised in Table 1.

2.2 Coupon tests

Five hourglass-shaped coupons were machined from the spare bolts of the same batch based on ASTM F606 and tested according to AS 1391 (2007). Specifically, two

unnotched coupons were tested to identify the engineering stress-strain curves. Three additional coupons with different notch sizes were tested to facilitate the subsequent numerical investigation on the fracture damage of high-strength bolts.

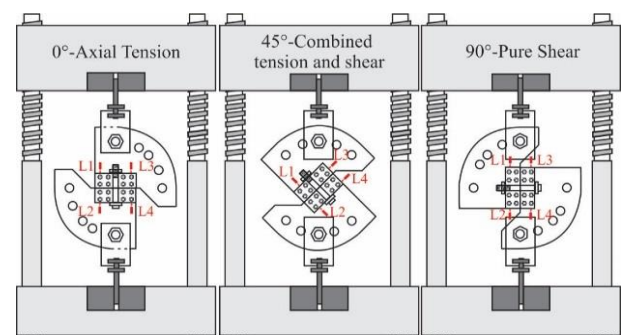
2.3 Test set-up and instrumentations

The specimens in the present study were tested with a 2000 kN capacity Dartec Machine at the University of Sydney. Pure tension and shear, as well as combined tension and shear were subjected to the tested bolts through rotating the testing rig by different loading angles (0° , 15° , 30° , 45° , 67.5° and 90°). The schematic and experimental view of the test specimens was illustrated in Fig. 3. As observed, two 36 mm high-strength steel rods (clamping bars) were placed within the grips such that the tested bolts underwent increasing deformations as the grips moved apart. A pinned joint of the testing rig ensured that no additional bending moments were transferred to the tested bolts. In addition, four linear variable differential transducers (LVDTs) were used to record the deformation of the tested bolt along and perpendicular to the bolt axis.

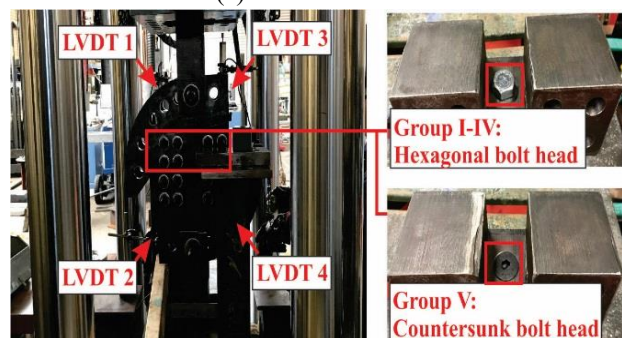
3. Experimental results

3.1 Material properties

The machined coupons were tested in a 300 kN machine with a loading rate of 0.5 mm/min. Axial elongation of each coupon was recorded by an extensometer with an initial gauge length of 25 mm. The full-range stress-strain curves of normal coupons without notches were shown in Fig. 4.



(a) Schematic view



(b) Photographic view

Fig. 3 Experimental setup

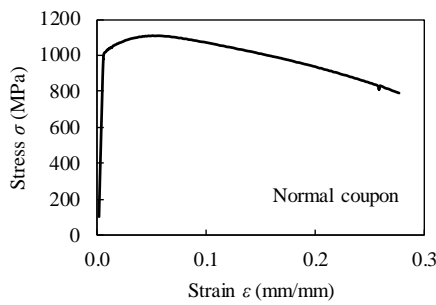
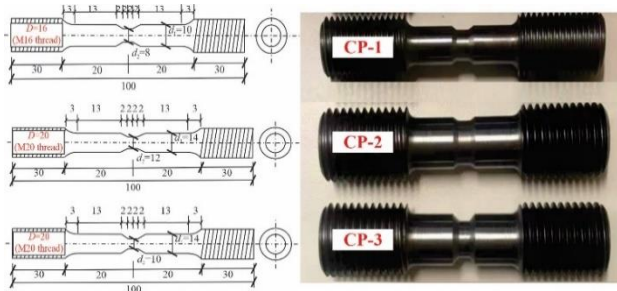
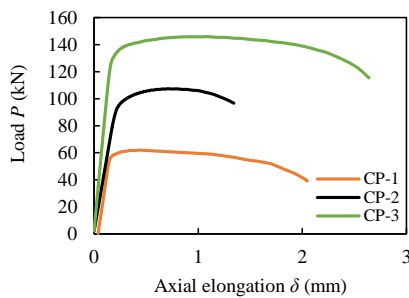


Fig. 4 Stress-strain relationships of Grade 10.9 bolts



(a) Schematic and photographic view of notched coupons



(b) Load-deformation curves

Fig. 5 Results of notched coupons

As shown, the average yield ($f_{0.2\%}$) and ultimate stress (f_u) for the Grade 10.9 bolts was 1013 MPa and 1100 MPa, which was about 10% higher than their characteristic values.

3.2 Notched coupon tests

In addition to the normal coupons without notches, three additional notched coupons with different notch sizes were included in the present test program (Fig. 5). Different triaxial stress states were obtained to identify their relationships with the fracture strains, which were used for the development of following numerical models. The load-deformation curves of notched coupons showed that the ductility after ultimate stress diminished with an increase of the notch size. It is noteworthy that the load-deformation curves of these notched coupons were only used for the calibration of the subsequent numerical model.

3.3 Plain bolt tests

3.3.1 Failure modes

As shown in Fig. 3, plain bolts of three various diameters have been tested under six loading angles until fracture. Each test was repeated three times to ensure the accuracy and reliability of the results. It should be noted that the threads of plain bolts were not included in the shear plane. The failure modes of tested plain bolts (M16, M20 and M24) were presented in Fig. 6, which were largely the same. In particular, the tested plain bolts under 0° and 15° failed by threads necking. No significant shear deformation within the bolt shank was observed, which was categorised as tension-led failure modes. On the other hand, the plain bolts tested under 30° to 90° experienced different degrees of shear deformation within the unthreaded shank, which meant this failure mode was dominated by shear forces.

3.3.2 Load-deformation curves

For the plain bolts with various diameters in Groups I-III, the load-deformation curves showed a similar trend and selected curves were presented in Fig. 7(a) for comparison purposes. In this study, plain bolts tested under 0° and 15° exhibited an initial linear part and followed by a transitional part until the ultimate load was achieved. The nonlinear response during the transitional part was from the yielding of the tested bolts. Thereafter, the applied loads decreased owing to the necking of threads until bolt fractured. The remaining plain bolts that were tested under 30° - 90° underwent a nonlinear transitional part after yielding was reached, which was followed by a plateau until shear fracture suddenly commenced. Test results in terms of the averaged ultimate strength capacity of each bolt were summarised in Table 2.

3.4 Set screw tests

3.4.1 Failure modes

Unlike the plain bolts, set screws are normally fully threaded through the screw shanks. Due to this inherent characteristic, the failure modes of set screws were different from those of plain bolts, especially when the screws were subjected to axial tension. As shown in Fig. 8(a), the tested set screws under 0° and 15° loading angles experienced significant plastic elongations. This was to be expected as the threaded proportions of set screws were significantly longer than those of the plain bolts, which inevitably resulted in greater elongations between the screw heads and nuts (clamping distance). On the other hand, the remaining set screws that were tested under 30° - 90° showed similar failure modes with the plain bolts.

3.4.2 Load-deformation curves

The load-deformation curves for set screws in Group IV are illustrated in Fig. 7(b), which show significantly different behaviour from those of plain bolts. As mentioned, set screws are fully threaded, which result in greater plastic deformations prior to fracture. This phenomenon was also demonstrated in the corresponding load-deformation curves, where the set screws under 0° and 15° loading angles



Fig. 6 Failure modes of plain bolts

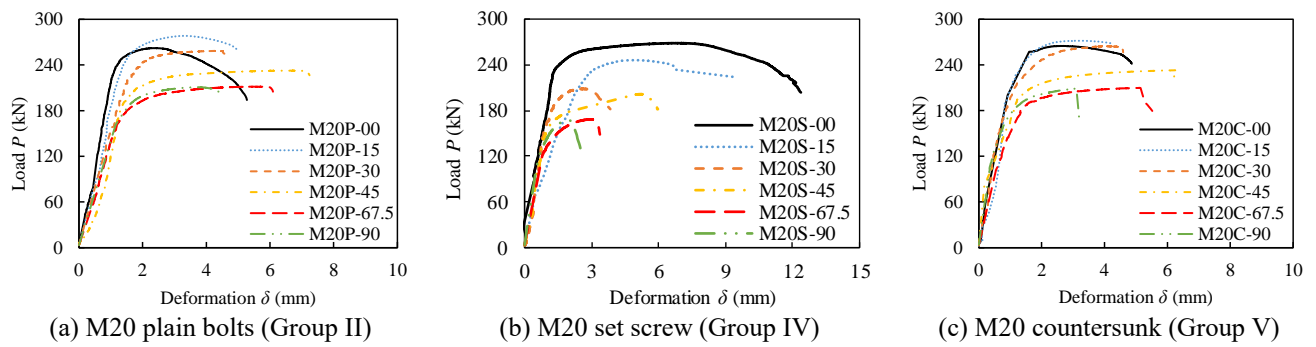


Fig. 7 Load-deformation curves of tested bolts



Fig. 8 Failure modes of set screw and countersunk bolts

Table 2 Test results of Grade 10.9 plain bolts (averaged values)

Tested Grade 10.9 bolts	Loading angles					
	0°	15°	30°	45°	67.5°	90°
P_U (kN)						
M16P (Group I)	168.1	180.2	169.0	151.1	135.8	136.2
M20P (Group II)	262.1	278.2	258.4	232.5	211.5	210.7
M24P (Group III)	384.8	401.8	376.8	337.2	311.3	316.8
M20S (Group IV)	268.5	246.1	208.5	181.5	159.0	169.9
M20C (Group V)	265.0	271.9	264.8	233.2	210.1	211.5

exhibited 12 mm and 9 mm deformations, which were nearly twice those of plain bolts. In addition, the set screws that were subjected to 30°-90° loading angles indicated less favoured shear resisting performance than that of plain

bolts. The maximum shear capacities and post-peak ductility performance were significantly lower than their counterparts in Group II.

3.5 Countersunk bolt tests

As shown in Fig. 8(b), bolt heads were sheared off for the countersunk bolts when tested under 0° and 15° loading angles. These failure modes are unique for structural bolts with countersunk head type, which are also different from those of plain bolts. The reason for this unique failure mode is due to the existence of socket recess, which reduces the stressed areas when the bolts are subjected to axial tension. However, the remaining countersunk bolts that are dominated by shear failure show similar final states with the normal plain bolts. This phenomenon is still to be expected as the stress concentration mainly occurs along the shear plane, which is not affected by the type of bolt head. Although the failure modes between plain bolts and countersunk bolts are slightly different, the load-deformation relationships of countersunk bolts in Group V are largely the same with those of plain bolts (Group II), as illustrated in Fig. 7(c). The difference in terms of the maximum tensile capacities and deformations at fracture between plain bolts and countersunk bolts are less than 5%.

3.6 Comparisons and discussions

In order to facilitate the comparison purposes, the ultimate loading capacity (P_U) of each tested bolt is normalised to its theoretical ultimate tensile capacity (P_0) at angle 0°. In particular, the theoretical ultimate tensile capacity (P_0) can be calculated with Eq. (1) as below

$$P_0 = f_{ub}A_s \quad (1)$$

$$A_s = \pi/4 (D - 0.9382P)^2 \quad (2)$$

where f_{ub} is the tensile stress of Grade 10.9 bolts and A_s is the actual tensile stress area of bolt shank with threads (AS1275, 1985). As observed in Fig. 9, the normalised ultimate loading capacities (P_U/P_0) of the tested plain bolts and countersunk bolt are similar at various loading angles. It is noteworthy that the normalised loading capacities of the tested bolts under 0° are 1.0, which are slightly smaller than those tested under 15° ($P_U/P_0=1.05$). For the plain bolts and countersunk bolts that experience more shear forces than tensile forces (67.5° and 90°), the normalised ultimate loading capacities are only around 0.8. As for set screws where the shanks are fully threaded, only the normalised axial tensile loading is the same with plain bolts and countersunk bolts.

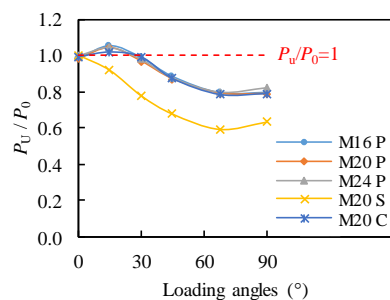


Fig. 9 Normalised capacities (P_U/P_0) versus loading angles

Once the shear force is included, the normalised loading capacities reduces to $P_U/P_0=0.6$ for those tested under pure shear.

4. Finite element analysis

4.1 General

Finite element analysis based on commercial software ABAQUS was employed herein to develop accurate numerical models for predicting the behaviour of high-strength structural bolts under different loading conditions. In the present study, Dynamic Explicit method was adopted due to its better capability to address the convergence issues than implicit method, as suggested by Thai *et al.* (2017). In addition, structural bolts were simulated with C3D8R element and 'surface-to-surface' contact was considered for all contacted surfaces. For the tangential direction, a friction coefficient of 0.3 between steel components was utilised (Li *et al.* 2016, 2018). It is noteworthy that the previous numerical models developed by Pavlović *et al.* (2013), Grimsmo *et al.* (2016) and Hu *et al.* (2016) included the bolt threads into consideration, which were less computational efficient due to the finer mesh regions near the bolt threads.

As suggested by Hedayat *et al.* (2017) and D'Aniello *et al.* (2017), this type of numerical model for structural bolt was not practical for the wider applications, where complicated joints (or frames) consisting of a large number of structural bolts were simulated. The authors herein thus proposed a simplified method to capture the behaviour of structural bolt, which can be readily applied into complicated numerical models. Specifically, the threaded shank was simplified to a reduced cross-sectional area A_s , which was about $0.78A_0$ according to Eq. (2). A general view of the model configuration was illustrated in Fig. 10. As observed, two reference points (RP-1 and RP-2) were assigned to the bottom and top clamping bars. The axial load (P) was applied to the top RP-2; whilst the bottom RP-1 was fixed.

4.2 Determination of material properties

The typical stress-strain behaviour of Grade 10.9 bolt (unnotched coupons) is shown in Fig. 4, which demonstrates its high-strength and superior ductility performance. The constitutive relationship of Grade 10.9 bolt is characterised by an initial linear response to 0.2% proof strength and continues with a nonlinear response until ultimate strength is attained. From this point, the accumulated strain energy starts to release, and the material gradually loses its strength until fracture is observed. As most of the traditional joint tests did not fail with bolt fracture, the high-strength bolts were simulated with bilinear or trilinear curves until ultimate strength (Shi *et al.* 2011). However, this type of model is not enough for the cases where structural bolts fail prior to the connected elements, such as the T-stubs tested by (Guo *et al.* 2017, Ribeiro *et al.* 2015) and the beam-to-column joint tests by (Coelho *et al.* 2004, Coelho and Bijlaard 2007, Wang *et al.*

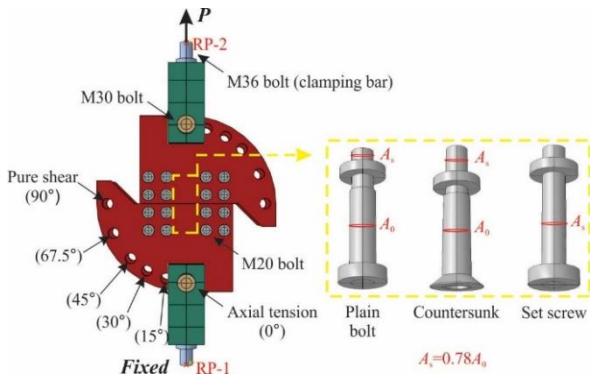


Fig. 10 Configuration of the developed finite element model

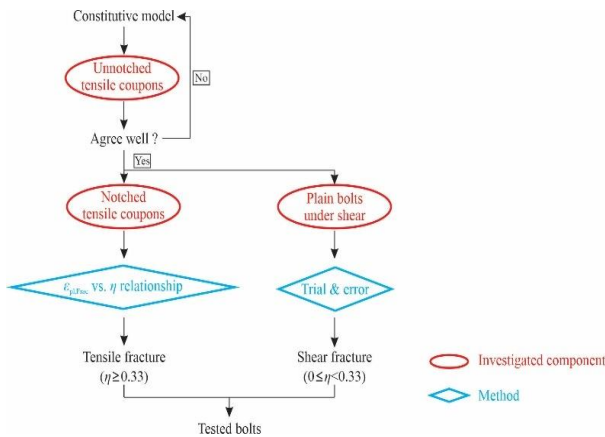


Fig. 11 Determination of the material properties

2018).

In order to simulate the full range behaviour of a typical bolted connection, where bolts are the weak components, comprehensive material properties accounting for fracture mechanism are included in this study. Three major steps were performed which included the identification of 1) constitutive model; 2) damage initiation; and 3) damage evolution. The detailed procedures are presented in a flow chart, as illustrated in Fig. 11.

4.2.1 Constitutive relationship

In the present study, three stress-strain curves are compared in Fig. 12(a), which include the engineering stress-strain curve, true stress-strain curve and proposed curve based on the true stress-strain curve. It is noteworthy that the engineering stress-strain curve was obtained from the unnotched coupon tests directly. The true stress-strain curve was adapted from the engineering stress-strain curve until the point where necking commenced. After the necking point, the perfect plastic range was extended until fracture strain (ε_f) is reached. As for the proposed 2-stage constitutive model, conventional true stress-strain curve was still adopted up to the necking point, and a modified power-law relationship that was proposed by Ling (1996) and successfully used by Song *et al.* (2020) was considered for the post-necking regime. As illustrated in Fig. 12(b), the utilisation of proposed 2-stage constitutive model (Eq. (3)) can better predict the post-peak behaviour of structural bolts.

$$\begin{aligned} \varepsilon_T &= \ln(1 + \varepsilon_E) \\ \sigma_T &= \sigma_E(1 + \varepsilon_E) & \varepsilon_T \leq \varepsilon_n \\ \sigma_T &= \sigma_n(\varepsilon_T/\varepsilon_n)^{\varepsilon_n} & \varepsilon_T > \varepsilon_n \end{aligned} \quad (3)$$

where ε_E , σ_E and ε_T , σ_T represented the engineering and true strain and stress, respectively; whilst ε_n and σ_n were the strain and stress at the point where necking commences.

The influences of using different stress-strain curves were investigated and compared against a selected tested bolt (M16-0°), which are presented in Fig. 12(b). As observed, the proposed 2-stage constitutive model predicts the post-peak softening behaviour of the selected bolt under axial tension very well.

4.2.2 Identification of damage initiation

In the present study, the tension and shear fracture of Grade 10.9 bolts were calibrated with the procedures and methods shown in Fig. 11. It is noteworthy that the bolt tensile fracture was identified through the notched coupon tests; whilst the shear fracture was determined comparing the test results and developed numerical models (Toribio and Ayaso 2003). Moreover, the damage model adopted herein was realised through ‘ductile damage’ in ABAQUS, where the relationship between the plastic strain at fracture ($\varepsilon_{pl,Frac}$) and stress triaxiality (η) was required.

For the identification of tensile fracture, the evolution history in terms of triaxiality and equivalent plastic strain for the most critical elements in tensile coupons were recorded through the developed numerical models, as shown in Fig. 13(a) with dashed lines. A skeleton curve was initially plotted by linking the fracture points of each tensile coupons. However, as the stress triaxiality of the critical element was not constant and changes significantly during the loading procedure (Bao and Wierzbicki 2004), the stress triaxiality at fracture point (η_u) cannot be utilised directly in the numerical simulations. A modified relationship between the equivalent plastic strain and averaged stress triaxiality of the critical elements was therefore developed based on Eq. (4).

$$\eta_{Ave} = \frac{\int_0^{\varepsilon_{pl,Frac}} \eta \times d\varepsilon_{pl}}{\varepsilon_{pl,Frac}} \quad (4)$$

in which η_{Ave} was the averaged stress triaxiality and $\varepsilon_{pl,Frac}$ was the equivalent plastic strain at fracture point. The relationship between the averaged stress triaxiality and equivalent plastic strain of the most critical elements is shown in Fig. 13(a). As observed, the locus of fracture strain ($\varepsilon_{pl,Frac}$) undergoes significant downward movement at medium stress triaxiality range (e.g. $0.33 < \eta < 0.8$).

By using the Johnson-Cook equation Eq. (5), a fitted exponential curve is developed when stress triaxiality is greater than 0.33.

$$\varepsilon_{pl,Frac} = D_1 + D_2 \exp(D_3 \eta_{Ave}) \quad \eta_{Ave} \geq 0.33 \quad (5)$$

where D_1 , D_2 and D_3 were calibrated as 0.25, 2.2 and -3.57 through mathematical regression method. As for the identification of shear fracture, it is difficult to machine shear coupons from the structural bolts.

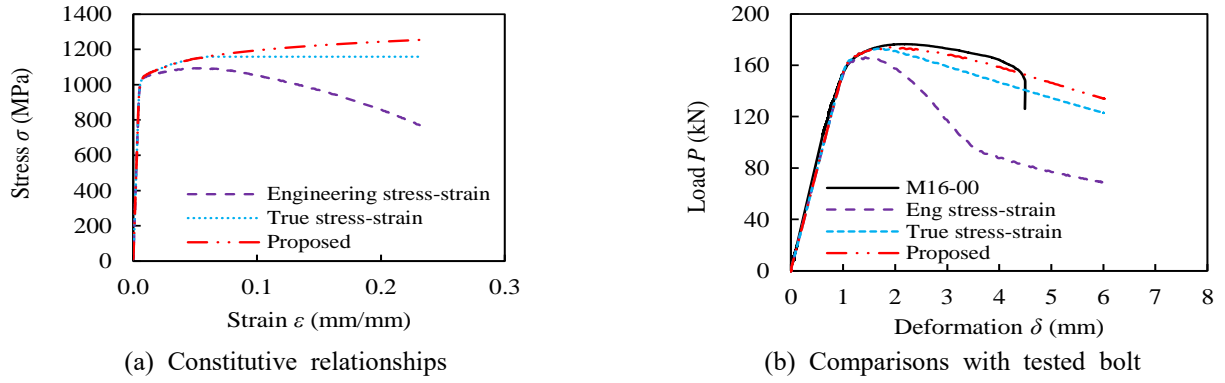


Fig. 12 Identification of constitutive model without damage

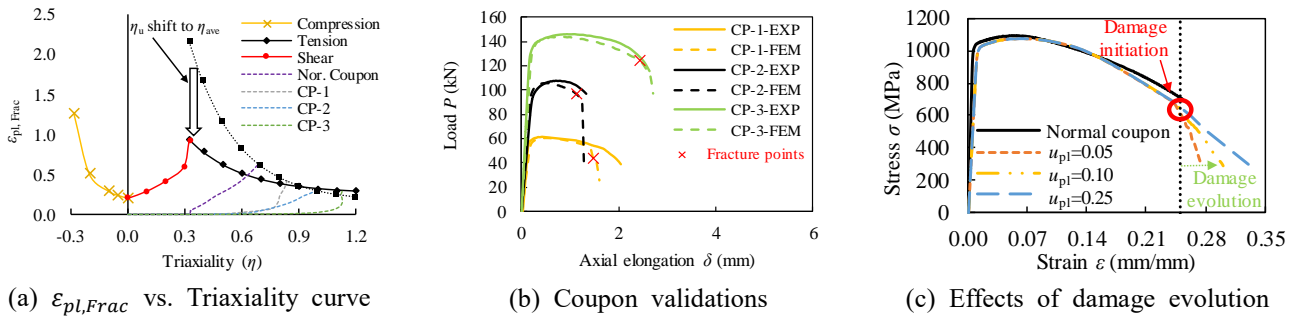


Fig. 13 Identification of damage initiation and evolution

The present study thus utilises a tested plain bolt under pure shear (M16-90°) to calibrate the relationship between the shear stress triaxiality and equivalent plastic strain at fracture. Eqs. (6) and (7) were used to characterise the shear fracture criterion under low stress triaxiality range, as illustrated in Fig. 13(a). In particular, D_4 and D_5 was calibrated as 0.2 and 3.6, respectively. With the tensile and shear fracture parameters calibrated, the full range behaviour of the tested coupons (including fracture points) can be mirrored accurately, as shown in Fig. 13(b).

$$\epsilon_{pl,Frac} = \frac{D_4}{(1 + 3\eta)}, \quad -0.33 < \eta \leq 0 \quad (6)$$

$$\epsilon_{pl,Frac} = D_4 \exp(D_5\eta) \quad 0 \leq \eta < 0.33 \quad (7)$$

4.2.3 Identification of damage evolution

Conventionally, the ductile damage evolution was closely related to the mesh size and need to be characterised to different values with a varied characteristic element length (u_{pl}). However, in the present study, the post-peak behaviour of the structural bolts was simulated with the full-range stress-strain relationship. The onset of fracture (both shear and tension) was simulated with the damage initiation, which was the focus of this study. On the other hand, the damage evolution only determined the rate of strength degradation after the damage initiation, which was less concerned herein. In order to obtain a more pronounced strength degradation so that the bolt fracture can be readily distinguished, a linear damage evolution with $u_{pl}=0.05$ mm was adopted (Fig. 13(c)).

4.3 Validation of the developed model

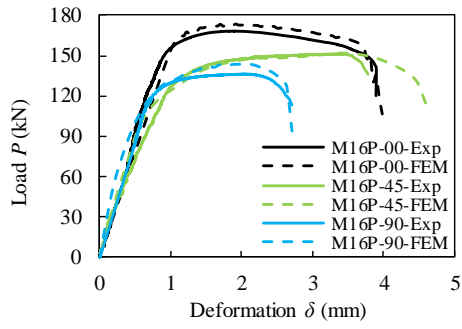
The structural bolts in each test group were utilised for the validation of the developed numerical models. Three loading conditions (0°, 45° and 90°) for each bolt type was selected for comparisons. As shown in Fig. 14, each tested bolt showed a similar and acceptable agreement in terms of the load-deformation curves between the experimental results and numerical analysis. In addition to the load-deformation curves, comparisons of the final state behaviour were also carried out. As observed, comparisons of failure modes for the tested bolts further demonstrated the accuracy of the proposed finite element model.

4.4 Parametric studies

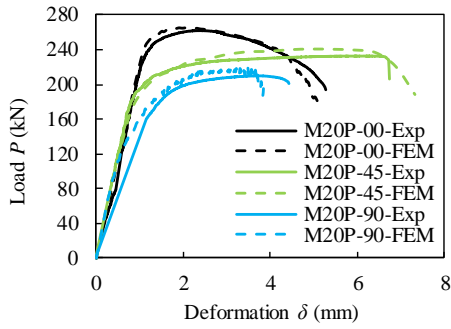
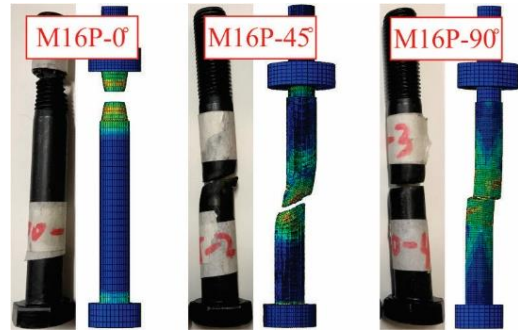
With the validated numerical model, the present study attempted to enhance the understanding of the behaviour of Grade 10.9 bolts through a series of parametric studies. As shown in Fig. 15, two practical parameters with the varied products available in the current market were considered herein, which included the ratio of threaded shank length over clamping distance (L_s/L_c), as well as the chamfer angle of the countersunk bolt (n°).

4.4.1 Effects of L_s/L_c (plain bolts)

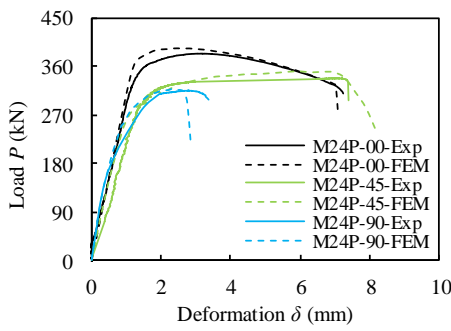
The effects of threaded shank length over clamping distance (L_s/L_c) were investigated herein with three values considered, which included 0.25, 0.5 and 0.75. As shown in Fig. 16(a), the effects of threaded proportion were mainly reflected in the axial elongations of the bolts; whilst the



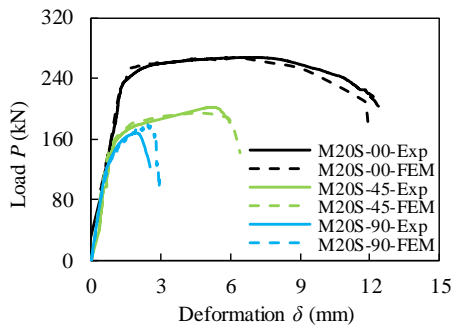
(a) Plain bolts M16P



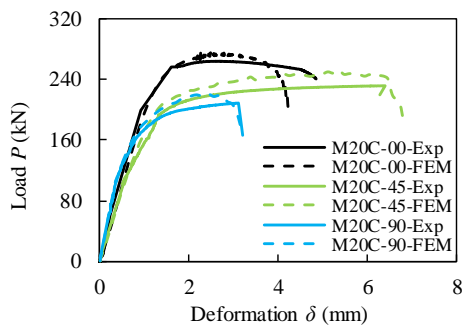
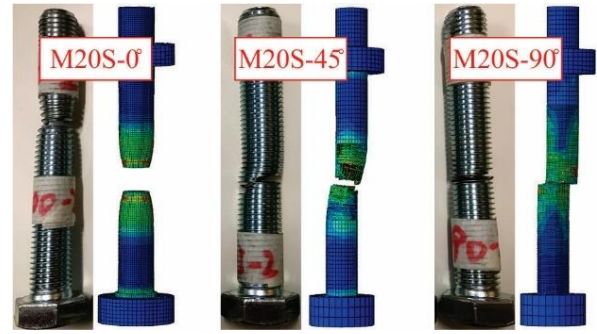
(b) Plain bolts M20P



(c) Plain bolts M24P



(d) Set screw M20S



(e) Countersunk bolts M20C

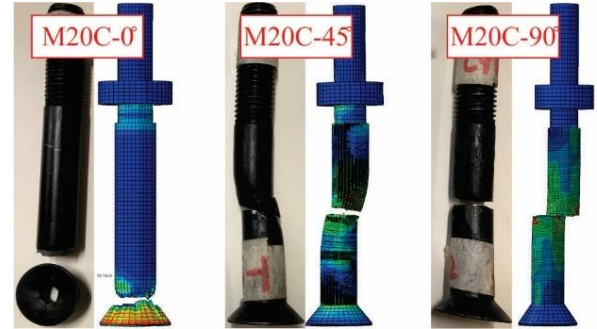


Fig. 14 Validation of the tested Grade 10.9 bolts

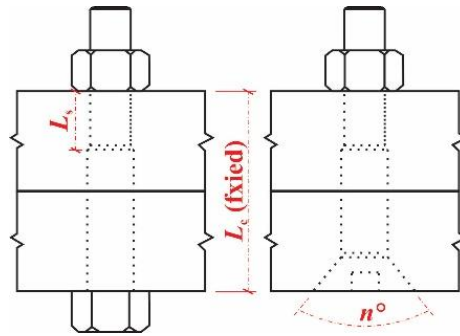


Fig. 15 Varied parameters for numerical analysis

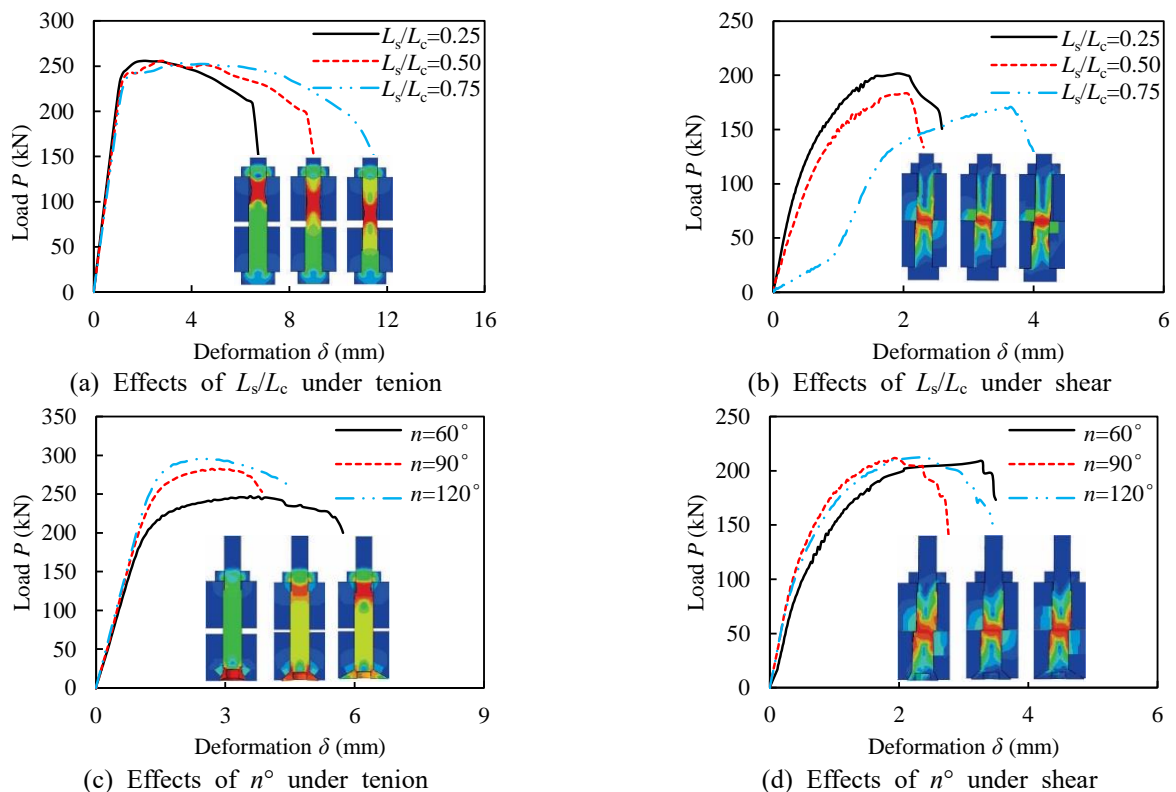


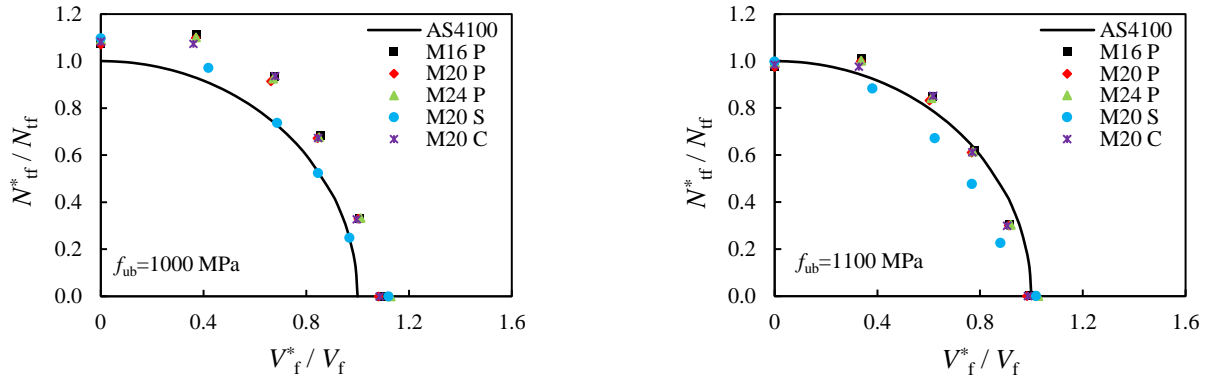
Fig. 16 Results of parametric study

tensile capacities of the investigated bolts were largely the same. The effects of L_s/L_c on the shear behaviour of plain bolts were illustrated in Fig. 16(b). As observed, the plain bolt with higher L_s/L_c exhibited lower shear capacity and more significant shear deformation. In particular, for those bolts where the shear plane passed through the unthreaded shank ($L_s/L_c=0.25$), full shear capacity was obtained. On the other hand, when the shear plane intercepted with the bolt threads ($L_s/L_c=0.75$), a reduced initial stiffness can be observed, which was mainly due to the bolt-hole clearance and the consequent slightly rotation of the bolt.

4.4.2 Effects of n° (countersunk bolts)

A countersunk bolt is normally utilised to ensure the bolt head can fit flush with the surface of the connected part. This type of structural bolt attracts increasing attention over the past few years, as it provides satisfactory

mechanical performance and meets aesthetic requirements. Countersunk bolts have a series of standard chamfer angles (60° , 82° , 90°), as well as some less popular chamfer angles (100° , 110° and 120°). In the present study, three chamfer angles (60° , 90° , 120°) that covered a wide range were selected. Moreover, to ensure the occurrence of bolt failure, rather than the failure of connected parts, the clamping distance was kept sufficient and constant in the following analysis ($L_c=100\text{mm}$). As shown in Figs. 16(c) and 16(d), the shear behaviour of countersunk bolts of different chamfer angles was similar, which meant that the effects of bolt head type on the shear performance was minimal and can be ignored. However, when the countersunk bolts were subjected to axial tension, the failure region shifted from bolt head to the threaded shank with an increase in the chamfer angle. In addition, the tensile capacity of the countersunk bolt also increased with an increase in the chamfer angle.



(a) with the nominal tensile strength

(b) with the actual tensile strength

Fig. 17 Comparisons of design strengths between the test results and AS 4100 (1998)

5. Comparison with current design standards

5.1. Current design methods

The existing design standards for steel structures that have been commonly used globally include AS 4100 (1998), Eurocode 3 (2005) and AISC 360 (2016). Among these international design provisions, Eurocode 3 (2005) and AISC 360 (2016) allow high-strength bolts of Grade 10.9 (or equivalent A490) to be used in the engineering practice; whilst Australian Standards AS 4100 (1998) only permits the structural bolts with a grade up to 8.8 to be utilised. The authors herein compared the strengths of the tested bolts with existing design provisions and corresponding design recommendations were provided.

5.1.1 AS 4100

The current Australian Standards for steel structures AS 4100 (1998) has limited the utilisation of high-strength bolts up to Grade 8.8. The authors herein compared the tested results with AS 4100 (1998) and the applicability of this design method was investigated. Pure shear and tension, as well as combined shear and tension capacity of a structural bolt at the ultimate limit state is defined in Eqs. (8)-(10). Safety reduction factors (ϕ and k_t) are taken as 1.0 herein for comparison. f_{ub} is identified as the ultimate tensile strength of the bolt. The number of shear planes with and without threads intercepting is represented by n_n and n_x , and A_c (equivalent to A_s) and A_0 is the minor and major diameter area of the bolt.

$$V_f = 0.62f_{ub}k_t(n_nA_c + n_xA_0) \quad (8)$$

$$N_{tf} = A_c f_{uf} \quad (9)$$

$$\left[\frac{V_f^*}{\phi V_f} \right]^2 + \left[\frac{N_{tf}^*}{\phi N_{tf}} \right]^2 \leq 1.0 \quad (10)$$

Comparison in terms of design strength between the test results and AS 4100 (1998) were performed, where both the nominal and actual tensile stress of Grade 10.9 bolts were used for the calculation of AS 4100 (1998). As specified, the nominal tensile stress of Grade 10.9 bolt was taken as 1000 MPa; whilst the actual tensile stress of Grade 10.9 bolt

(1100 MPa) was determined through the unnotched coupon tests in Section 3.1. With the actual design value utilised, AS 4100 (1998) predicted 5%-10% higher loading capacities for the set screws under combined loading conditions (Fig. 17), which were not safe for the design purposes.

5.1.2 Eurocode 3

Shear and tension resistance of the structural bolts are defined in Eurocode 3 (2005) through Eqs. (11) and (12), respectively

$$F_{v,Rd} = \alpha_v f_{ub} A / \gamma_{M2} \quad (11)$$

$$F_{t,Rd} = k_2 f_{ub} A_s / \gamma_{M2} \quad (12)$$

in which α_v is the reduction factor for the bolts under shear forces and is defined as 0.5 and 0.6 when the shear plane passes through the threaded and unthreaded bolt shanks, respectively. Similarly, A is defined as the shear stress area and should be taken as A_s or A_0 , when the shear plane passes through the threaded and unthreaded proportion of the bolt. Moreover, Eurocode 3 (2005) is the only design standard that distinguishes the bolt tensile capacities according to their bolt head type. Reduction factor k_2 which accounts for the variation of bolt head is included for the tensile strength prediction. As specified, k_2 was taken as 0.63 for countersunk bolt; whilst a coefficient of 0.9 was assigned for the remaining bolt head types. It is noteworthy that the safety factors were defined as 1.25 for the design of structural bolts. However, this coefficient was taken as unity herein so that the comparisons in terms of the ultimate loading capacities with the test results can be carried out. In addition, Eq. (13) was proposed for the structural bolts that were subjected to combined shear and tension, where coefficient 1.4 was included into the tension component to conservatively account for the capacity enhancement when the bolts were subjected to 15° angle.

$$\frac{F_{v,Ed}}{F_{v,Rd}} + \frac{F_{t,Ed}}{1.4F_{t,Rd}} \leq 1.0 \quad (13)$$

Comparison of design strength between the test results and Eurocode 3 (2005) are shown in Fig. 18. As observed, Eurocode 3 (2005) produced conservative yet acceptable design capacities for the plain bolts and set screws when the

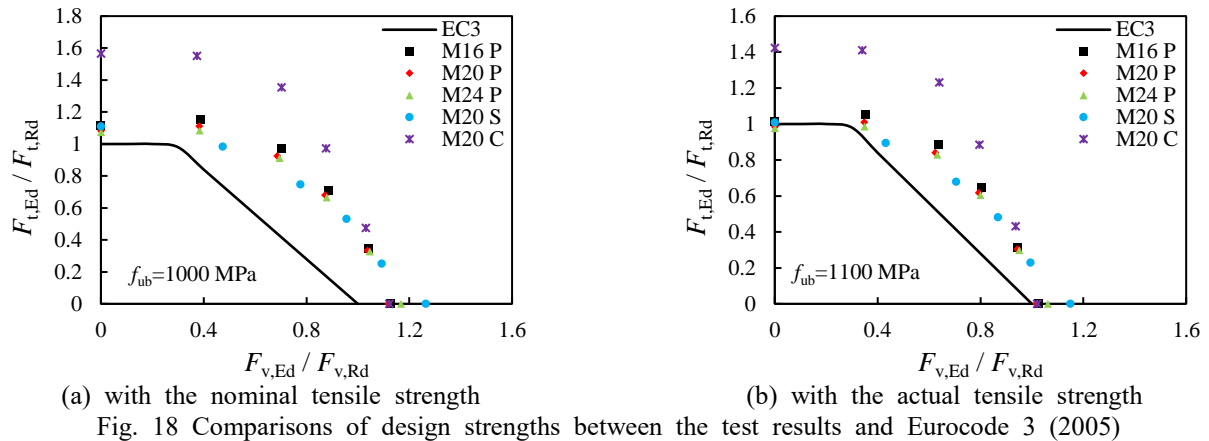


Fig. 18 Comparisons of design strengths between the test results and Eurocode 3 (2005)

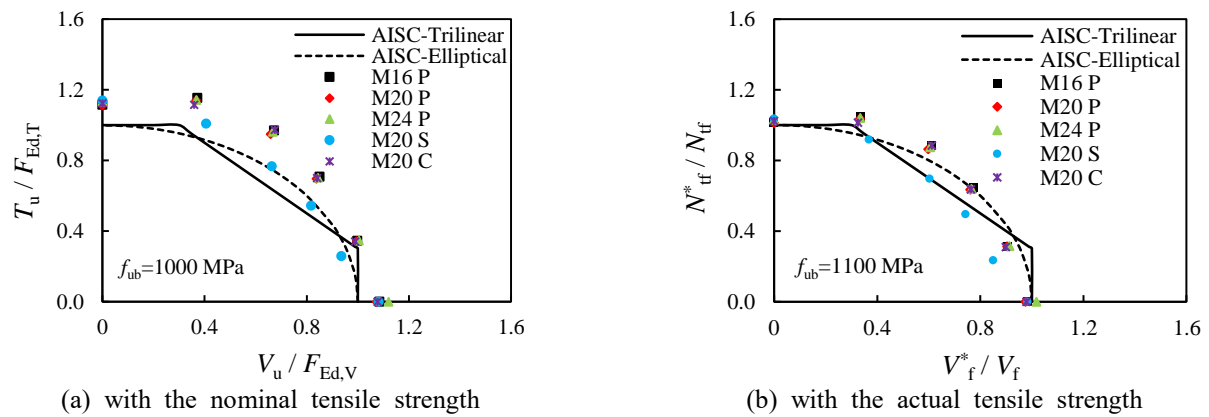


Fig. 19 Comparisons of design strengths between the test results and AISC 360 (2016)

actual tensile strength was adopted. This design method included the effects of strength enhancement when the bolts were subjected to a small proportion of shear forces. However, as the loading capacities of the bolts did not decrease linearly with an increase of loading angles, Eurocode 3 (2005) produced relatively conservative predictions for the bolt strength when the loading angles ranged from 30° to 67.5° . Besides, the most significant limitation of Eurocode 3 (2005) was the over-conservative tensile strength for the countersunk bolts, which resulted in unnecessary design redundancy in the engineering practice.

5.1.3 AISC 360-16

American Standards provided the Load and Resistance Factor Design (LRFD) design rules for structural joints using high-strength bolts. The design strength (F_{Ed}) in shear or tension for an ASTM A490 (equivalent to Grade 10.9) high-strength bolt was specified as Eq. (14)

$$F_{Ed} = \phi f_{ub} A_b \quad (14)$$

where f_{ub} and A_b was the nominal strength per unit area and cross-sectional area based on the nominal bolt diameter. The determination of f_{ub} depends on the grade of structural bolt and type of loading. The design strength safety reduction factor (ϕ) was defined as 0.75 and once again was neglected herein for comparison purposes. When combined shear and tension loads were transmitted by an ASTM A490

bolt, the AISC 360 (2016) specified that the limit-state interaction should satisfy either Eq. (15(a)) or Eq. (15(b)).

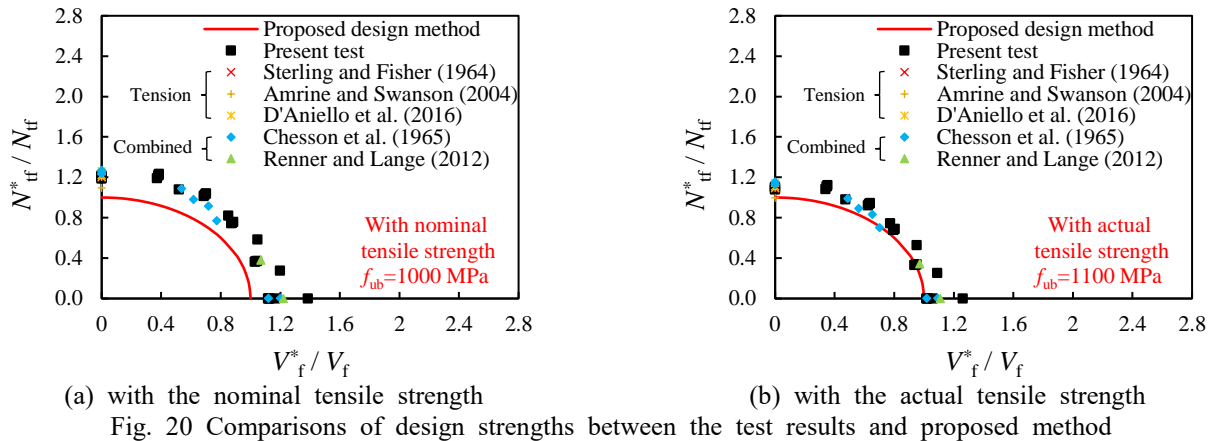
$$\left[\frac{V_u}{\phi F_{Ed,V}} \right]^2 + \left[\frac{T_u}{\phi F_{Ed,T}} \right]^2 \leq 1.0 \quad (15a)$$

$$F'_{nt} = 1.3F_{nt} - F_{nt} f_{rv} / \phi F_{nv} \quad (15b)$$

Fig. 19 presents the comparisons between the test results and analytical values specified in AISC 360 (2016). As observed, AISC 360 (2016) produced accurate strength predictions for the tested A490 bolts under pure tension and shear. However, predictions for the A490 bolts under combined tension and shear were not safe, which was particularly prominent for the fully threaded set screws.

5.2 Design recommendations

The bilinear curve adopted in Eurocode 3 (2005) was based on two sets of test data, which were performed in the 1970s on lower strength bolts. For conservative reasons, Eurocode 3 (2005) limited all the test results within the skeleton curve and achieved design safety by sacrificing the bolt strength under combined shear and tension. However, with the improvement of manufacturing, the quality of the bolt has been demonstrated through the present experimental test. It is therefore necessary to develop an accurate and safe design method for the high-strength structural bolts of Grade 10.9.



The authors herein adapted design Eqs. (16) and (17) to predict the shear and tension resistance for different types of structural bolts of Grade 10.9. In particular, Eq. (16) lowered the shear reduction factor to 0.6 and 0.5 for structural bolts, where the shear plane passed through the unthreaded and threaded bolt shanks, respectively. It should be noted that for most of the design standard users, the actual ultimate tensile stress (f_{ub-act}) of structural bolts were not available. The nominal ultimate tensile stress (f_{ub-nom}) of Grade 10.9 bolts was therefore suggested for the possible inclusion of existing design standards, which was 1000 MPa. With respect to the tensile capacity, a reduction factor of 0.9 was suggested for Grade 10.9 bolts. For the structural bolts that were subjected to both shear and tension, the design limitation specified in AS 4100 (1998) can be adopted, through which the unnecessary design redundancy can be avoided.

$$V_f = 0.6f_{ub}A_0 \quad (\text{Shear plane in unthreaded shank}) \quad (16)$$

$$V_f = 0.5f_{ub}A_c \quad (\text{Shear plane in threaded shank})$$

$$N_{tf} = 0.9A_c f_{ub} \quad (17)$$

The present and previous test results were collected and compared with the proposed design method, as shown in Fig. 20. Most of the previous test results on Grade 10.9 bolts focused on the tensile strength only. Only limited tests were conducted to investigate the Grade 10.9 bolts with partially threaded shank and hexagonal heads under combined actions. As observed, the proposed design equations were reasonably conservative when the nominal bolt tensile strength was used by structural engineers. With the safety reduction factors being included, an appropriate level of design redundancy can be maintained. Moreover, even with the actual bolt tensile strength being identified and utilised, the predicted strength capacities were still accurate and on the safe side, as shown in Fig. 20(b). It is noted that the development of design standards should be based on the actual material properties of the tested specimens with all the reduction factors set as unity. Therefore, Figs. 17(b), 18(b) and 19(b) should be the ones used for comparisons and development of design specification. As observed, the current design standards result in accurate predictions for bolt strength under tension and shear (except for Eurocode 3 for countersunk bolts).

Nevertheless, none of these design specifications can safely and accurately predict the bolt strength under a larger proportion of shear force, such as the loading angle of 45° and 67.5° . Considering the less favoured ductility performance of high-strength steel bolts, the proposed method, therefore, intentionally underestimates the bolts' tensile strength by 10% to achieve a conservative design envelop for the bolts under combined actions, which is similar to the development of Eurocode 3 (2005).

6. Conclusions

An experimental study consisting of five different types of Grade 10.9 structural bolts was conducted. Unnotched coupons were extracted from the spare bolts and tested to ascertain the basic constitutive relationship for Grade 10.9 bolts. Additional notched coupons of different sizes were also tested to identify the relationship between the plastic strain and stress triaxiality, which was further used for the calibration of fracture model. In addition to the experimental tests, finite element model based on ABAQUS was developed to simulate the full-range behaviour of structural bolts under different loading combinations. Furthermore, the strength limit state behaviour of the tested bolts was compared with the existing design provisions and the corresponding design recommendations were provided. The following conclusions were drawn by comparing the test results and existing codes of practice:

- Grade 10.9 plain bolts and countersunk bolts that are subjected to 15° loading angle exhibit 5% higher tensile strength than those tested under 0° loading angle. As for the Grade 10.9 set screws, the strength capacity decreases gradually when increasing the loading angle from 0° to 90° .
- Shear strength of structural bolts closely relates to the shear plane. Generally, shear capacity of Grade 10.9 bolt is around 80% and 60% of its tension capacity when the shear plane passes through the unthreaded and threaded shank, respectively.
- Tensile and shear performance of countersunk bolts is similar to plain bolts in terms of the strength capacity and ultimate elongation (or shear deformation). A further reduction factor of 0.63 in European Standards

might not be necessary.

- A full-range fracture model (for both shear and tension fracture) is developed in the present study. The accuracy of the developed model is validated successfully, which indicates that this model can be further utilised for the simulation of typical joints in steel and composite structures.
- A modified design method is developed in the present study, through which the tensile and shear capacity of Grade 10.9 bolts (of various types) can be accurately predicted and safely utilised for the engineering practice.

Acknowledgments

The first author was financially supported by the Australian Research Council (ARC) under its Discovery Scheme (Project No: DP170100001). Assistance from Dr Mohanad Mursi and staff of Centre for Advanced Structural Engineering (CASE) at the J.W. Roderick Laboratory are gratefully acknowledged.

References

- Amrine, J.J. and Swanson, J.A. (2004), "Effects of variable pretension on the behavior of bolted connections with prying," *Engineering Journal*, American Institute of Steel Construction, 3rd Quarter, 2004.
- ANSI/AISC 360-16 (2016), Specification for structural steel buildings. Chicago: AISC.
- ASTM Standard F606 (2016), Standard Test Methods for Determining the Mechanical Properties of Externally and Internally Threaded Fasteners, Washers, Direct Tension Indicators, and Rivets, ASTM International, West Conshohocken, PA, 2003 https://doi.org/DOI:10.1520/F0606_F0606M-16.
- AS 1391 (2007), Metallic materials-Tensile testing at ambient temperature. Standards Australia.
- AS 1275 (1985), Metric screw threads for fasteners. Standards Australia.
- Bao, Y. and Wierzbicki, T. (2004), "On fracture locus in the equivalent strain and stress triaxiality space", *Int. J. Mech. Sci.*, **46**, 81-98. <https://doi.org/10.1016/j.ijmecsci.2004.02.006>
- Cai, Y. and Young, B. (2019), "Experimental investigation of carbon steel and stainless steel bolted connections at different strain rates", *Steel Compos. Struct.*, **30**(6), 551-565. <https://doi.org/10.12989/scs.2019.30.6.551>.
- Chesson, E., Faustino, N.L. and Munse, W.H. (1965), "High-strength bolts subjected to tension and shear", *J. Struct. Div. ASCE*, **91**(5), 155-180.
- Coelho, A.M.G., Bijlaard, F. and Simões da Silva, L. (2004), "Experimental assessment of the ductility of extended end plate connections", *Eng. Struct.*, **26**(9), 1185-1206. <https://doi.org/10.1016/j.engstruct.2000.09.001>.
- Coelho, A.M.G. and Bijlaard, F. (2007), "Experimental behaviour of high strength steel end-plate connections", *J. Constr. Steel Res.*, **63**: 1228-1240. <https://doi.org/10.1016/j.jcsr.2006.11.010>.
- D'Anello, M., Cassiano, D. and Landolfo, R. (2016), "Monotonic and cyclic inelastic tensile response of European preloadable gr10.9 bolt assemblies", *J. Constr. Steel Res.*, **124**: 77-90. <https://doi.org/10.1016/j.jcsr.2016.05.017>
- D'Anello, M., Cassiano, D. and Landolfo, R. (2017), "Simplified criteria for finite element modelling of European preloadable bolts", *Steel Compos. Struct.*, **24**(6), 643-658. <https://doi.org/10.12989/scs.2017.24.6.643>.
- Ding, F.X., Yin, G.A., Wang, H.B., Wang, L. and Guo, Q. (2017), "Behavior of headed shear stud connectors subjected to cyclic loading", *Steel Compos. Struct.*, **25**(6), 705-716. <https://doi.org/10.12989/scs.2017.25.6.705>.
- Du, Y., Chen, Z., Liew, J.Y.R. and Xiong, M.X. (2017), "Rectangular concrete-filled steel tubular beam-columns using high-strength steel: Experiments and design", *J. Constr. Steel Res.*, **131**, 1-18. <https://doi.org/10.1016/j.jcsr.2016.12.016>.
- Ebrahimi, S., Zahrai, S.M. and Mirghaderi, S.R. (2019), "Numerical study on force transfer mechanism in through gusset plates of SCBFs with HSS columns & beams", *Steel Compos. Struct.*, **31**(6), 541-558. <https://doi.org/10.12989/scs.2019.31.6.541>.
- EI-Lobody, E. and Lam, D. (2002), "Modelling of headed stud in steel-precast composite beams", *Steel Compos. Struct.*, **2**(5): 355-378. <https://doi.org/10.12989/scs.2002.2.5.355>.
- Eurocode 3 (2005), Design of Steel Structures, Part 1.8: Design of joints. BS EN 1993-1-8, (London, UK; 2005).
- European Committee for Standardization (CEN) (2005), EN 14399-3-High Strength Structural Bolting for Preloading-Part 3: System HR - Hexagon Bolt and Nut Assemblies.
- Francavilla, A., Latour, M., Piluso, V. and Rizzano, G. (2016), "Bolted T-stubs: A refined model for flange and bolt fracture modes", *Steel Compos. Struct.*, **20**(2), 267-293. <https://doi.org/10.12989/scs.2016.20.2.267>.
- Grimsmo, E.L., Aalberg, A., Langseth, M. and Clausen, A.H. (2016), "Failure modes of bolt and nut assemblies under tensile loading", *J. Constr. Steel Res.*, **126**, 15-25. <https://doi.org/10.1016/j.jcsr.2016.06.023>.
- Guo, H., Liang, G., Li, Y. and Liu, Y. (2017), "Q690 high strength steel T-stub tensile behavior Experimental research and theoretical analysis", *J. Constr. Steel Res.*, **139**, 473-483. <https://doi.org/10.1016/j.jcsr.2017.10.007>.
- Hedayat, A.A., Afzadi, E.A. and Iranpour, A. (2017), "Prediction of the bolt fracture in shear using finite element method", *Structures*, **12**, 188-210. <https://doi.org/10.1016/j.istruc.2017.09.005>.
- Hou, Z., Xia, H. and Zhang, Y. (2012), "Dynamic analysis and shear connector damage identification of steel-concrete composite beams", *Steel Compos. Struct.*, **13**(4), 327-341. <https://doi.org/10.12989/scs.2012.13.4.327>
- Hu, Y., Shen, L., Nie, S., Yang, B. and Sha, W. (2016), "FE simulation and experimental tests of high-strength structural bolts under tension", *J. Constr. Steel Res.*, **126**, 174-186. <https://doi.org/10.1016/j.jcsr.2016.07.021>.
- Huang, Z., Huang, X., Li, W., Mei, L. and Liew, J.Y.R. (2019), "Experimental behavior of VHSC encased composite stub column under compression and end moment", *Steel Compos. Struct.*, **31**(1), 69-83. <https://doi.org/10.12989/scs.2019.31.1.069>.
- ISO (2009), ISO Mechanical properties of fasteners made of carbon steel and alloy steel, Part 1: Bolts, screws and studs with specified property classes - Coarse thread and fine pitch thread.
- Kawohl, A.K. and Lange, J. (2016), "Tests on 10.9 bolts under combined tension and shear", *Acta Polytechnica*, **56**(2), 112-117. <https://doi.org/10.14311/asfe.2015.050>.
- Ketabdari, H., Daryan, A.S. and Hassani, N. (2019), "Predicting post-fire mechanical properties of grade 8.8 and 10.9 steel bolts", *J. Constr. Steel Res.*, **162**, 105735. <https://doi.org/10.1016/j.jcsr.2019.105735>.
- Lange, J. and González, F. (2012), "Behavior of high-strength grade 10.9 bolts under fire conditions", *Struct. Eng. Int.*, **4**, 470-475. <https://doi.org/10.2749/101686612X13363929517451>
- Li, D., Uy, B. and Wang, J. (2019), "Behaviour and design of high-

- strength steel beam-to-column joints”, *Steel Compos. Struct.*, **31**(3), 303-317. <https://doi.org/10.12989/scs.2019.31.3.303>.
- Li, D., Uy, B., Patel, V. and Aslani, F. (2016), “Analysis and design of demountable embedded steel column base connections”, *Steel Compos. Struct.*, **22**(2), 429-448. <https://doi.org/10.12989/scs.2016.22.4.753>.
- Li, D., Uy, B., Patel, V. and Aslani, F. (2018), “Behaviour and design of demountable CFST column-column connections subjected to compression”, *J. Constr. Steel Res.*, **141**, 262-274. <https://doi.org/10.1016/j.jcsr.2017.11.021>.
- Li, X., Zhou, X., Liu, J. and Wang, X. (2019), “Shear behavior of short square tubed steel reinforced concrete columns with high-strength concrete”, *Steel Compos. Struct.*, **32**(3), 411-422. <https://doi.org/10.12989/scs.2019.32.3.411>.
- Ling, Y. (1996), “Uniaxial true stress-strain after necking”, *AMP J. Technol.*, **5**(1), 37-48.
- Long, L., Yan, S., Gao, X. and Kang, H. (2016), “Three-dimensional finite element simulation and application of high-strength bolts”, *Steel Compos. Struct.*, **20**(3), 501-512. <https://doi.org/10.12989/scs.2016.20.3.501>.
- Ma, J.L., Chan, T.M. and Young, B. (2018), “Design of cold-formed high-strength steel tubular stub columns”, *J. Struct. Eng.*, **144**(6), 04018063. [https://doi.org/10.1061/\(ASCE\)ST.1943-541X.0002046](https://doi.org/10.1061/(ASCE)ST.1943-541X.0002046).
- Nah, H.S. and Choi, S.M. (2017), “Estimation on clamping load of high strength bolts considering various environment conditions”, *Steel Compos. Struct.*, **24**(4), 399-408. <https://doi.org/10.12989/scs.2017.24.4.399>.
- Nair, R.S., Birkemoe, P.C. and Munse, W.H. (1974). “High strength bolts subject to tension and prying,” *J. Struct. Div., ASCE*, **100**(2), 351-372.
- Pavlović, M., Marković, Z., Veljković, M. and Budevc, D. (2013), “Bolted shear connectors vs. headed studs behaviour in push-out tests”, *J. Constr. Steel Res.*, **88**, 134-149. <https://doi.org/10.1016/j.jcsr.2013.05.003>.
- Qi, J., Wang, J., Li, M. and Chen, L. (2017), “Shear capacity of stud shear connectors with initial damage: Experiment, FEM model and theoretical formulation”, *Steel Compos. Struct.*, **25**(1), 79-92. <https://doi.org/10.12989/scs.2017.25.1.079>.
- Rehman, N., Lam, D., Dai, X. and Ashour, A.F. (2016), “Experimental study on demountable shear connectors in composite slabs with profiled decking”, *J. Constr. Steel Res.*, **122**, 178-189. <https://doi.org/10.1016/j.jcsr.2016.03.021>.
- Renner, A. and Lange, J. (2012), “Load-bearing behavior of high-strength bolts in combined tension and shear”, *Steel Constr.*, **5**(3), 151-157. <https://doi.org/10.1002/stco.201210019>.
- Ribeiro, J., Santiago, A., Rigueiro, C. and Simões da Silva, L. (2015), “Analytical model for the response of T-stub joint component under impact loading”, *J. Constr. Steel Res.*, **106**, 23-34. <https://doi.org/10.1016/j.jcsr.2014.11.013>.
- Shamass, R. and Cashell, K.A. (2017), “Behaviour of composite beams made using high strength steel”, *Structures*, **12**, 88-101. <https://doi.org/10.1016/j.istruc.2017.08.005>.
- Shi, Y., Wang, M. and Wang, Y. (2011), “Analysis on shear behaviour of high-strength bolts connection”, *Int. J. Steel Struct.*, **11**(2), 203-213. <https://doi.org/10.1007/s13296-011-2008-0>.
- Song, Y., Wang, J., Uy, B. and Li, D. (2020), “Experimental behaviour and fracture prediction of austenitic stainless steel bolts under combined tension and shear”, *J. Constr. Steel Res.*, **166**, 105916. <https://doi.org/10.1016/j.jcsr.2019.105916>.
- Sterling, G.H. and Fisher, J.W. (1964). “Tests of A490 Bolts.” Fritz Engineering Lab. Report, No. 288.15, Lehigh University.
- Standards Australia, AS 4100-1998: Steel structures, 2016.
- Thai, H.T., Vo, T.P., Nguyen, T.K. and Pham, C.H. (2017), “Explicit simulation of bolted endplate composite beam-to-CFST column connections”, *Thin-Wall. Struct.*, **119**, 749-759. <https://doi.org/10.1016/j.tws.2017.07.013>.
- Toribio, J. and Ayaso, F.J. (2003). “A fracture criterion for high-strength steel structural members containing notch-shape defects”. *Steel Compos. Struct.*, **3**(4), 231-242. <https://doi.org/10.12989/scs.2003.3.4.231>.
- Uy, B. (2001), “Strength of short concrete filled high strength steel box columns”, *J. Constr. Steel Res.*, **57**, 113-134. [https://doi.org/10.1016/S0143-974X\(00\)00014-6](https://doi.org/10.1016/S0143-974X(00)00014-6).
- Vasdravellis, G., Karavasilis, T.L. and Uy, B. (2014), “Design rules, experimental evaluation, and fracture models for high-strength and stainless-steel hourglass shape energy dissipation devices”, *J. Struct. Eng.*, **140**(11), 04014087. [https://doi.org/10.1061/\(ASCE\)ST.1943-541X.0001014](https://doi.org/10.1061/(ASCE)ST.1943-541X.0001014).
- Wang, F., Zhao, O. and Young, B. (2020), “Testing and numerical modelling of S960 ultra-high strength steel angle and channel section stub columns”, *Eng. Struct.*, **204**, 109902. <https://doi.org/10.1016/j.engstruct.2019.109902>.
- Wang, J. and Sun, Q. (2019), “Seismic behavior of Q690 circular HCFTST columns under constant axial loading and reversed cyclic lateral loading”, *Steel Compos. Struct.*, **32**(2), 199-212. <https://doi.org/10.12989/scs.2019.32.2.199>.
- Wang, J., Uy, B., Thai, H.T. and Li, D. (2018), “Behaviour and design of demountable beam-to-column composite bolted joints with extended end-plates”, *J. Constr. Steel Res.*, **144**, 221-235. <https://doi.org/10.1016/j.jcsr.2018.02.002>.
- Yan, J. B., Wang, Z., Wang, T. and Wang, X.T. (2018), “Shear and tensile behaviors of headed stud connectors in double skin composite shear wall”, *Steel Compos. Struct.*, **26**(6), 759-769. <https://doi.org/10.12989/scs.2018.26.6.759>.
- Yang, J., Sheehan, T., Dai, X. and Lam, D. (2017), “Structural behaviour of beam to concrete-filled elliptical steel tubular column connections”, *Structures*, **9**, 41-52. <https://doi.org/10.1016/j.istruc.2016.09.005>.
- Zhao, H. and Yuan, Y. (2010), “Experimental studies on composite beams with high-strength steel and concrete”, *Steel Compos. Struct.*, **10**(5), 373-383. <https://doi.org/10.12989/scs.2010.10.5.373>.

DL